RSC Advances

ROYAL SOCIETY OF CHEMISTRY

www.rsc.org/advances

Cite this: DOI: 10.1039/c0xx00000x

www.rsc.org/xxxxxx

ARTICLE TYPE

Preparation of Fe/activated carbon directly from rice husk pyrolytic carbon and its application in catalytic hydroxylation of phenol

Xian Zhang, Yaxin Li, Guiying Li*, Changwei Hu*

Received (in XXX, XXX) Xth XXXXXXXXX 20XX, Accepted Xth XXXXXXXXX 20XX

DOI: 10.1039/b000000x

Rice husk pyrolytic carbon (PC) was pretreated by NaOH solution at 100 °C for 5 h to remove SiO_2 and then used to prepare Fe/activated carbon catalyst. The treated sample was impregnated with ferric nitrate solution, and then activated under N_2 atmosphere, obtaining Fe/activated carbon catalysts. The samples were characterized by temperature programed decomposition-mass spectra (TPD-MS), Brauner-Emmett-Teller (BET), inductively coupled plasma atomic emission spectrometry (ICP-AES), scanning electron microscopy (SEM), X-ray diffraction (XRD), and X-ray photoelectron spectroscopy (XPS). The specific surface area increased with activation temperature until 750 °C. With the increase of iron content, the specific surface area of carbon increased first up to 0.39 mmol/g iron loaded and then decreased. Reactive decomposition of ferric nitrate happened at 120-350 °C releasing NO and CO_2. Part of ferric (Fe(III)) species was reduced to ferrous (Fe(II)) species forming Fe_3O_4 at 400-550 °C, and metal Fe at 650-750 °C. The Fe/activated carbon exhibited high activity and selectivity for phenol hydroxylation.

1. Introduction

Rice husk (RH) is an agricultural residue abundantly available in rice-producing countries. The annual worldwide output has been estimated to be 80 million tons, of which about a half is generated in China [1]. However, rarely researches concerning its utilization are carried out. If this agricultural residue is not utilized properly, tremendous waste will be produced, causing energy loss and environmental pollution. Rice husk has been used to produce bio oil via pyrolysis [2], with the production of a lot of rice husk powder, pyrolytic carbon (PC), as the by-product. The preparation of activated carbon from agricultural residue can not only reduce environmental pollution but also reduce the cost of activated carbon production. It has great research value to use PC to prepare activated carbon. This can simultaneously provide ways to solve the problem of pollution and take full advantage of raw material, that is, the components of rice husk are totally used, producing both energy material (bio-oil) and useful AC.

Functionalized and metal impregnated activated carbons (ACs) were promising catalysts and sorbents for various industrial applications. For example, iron containing catalysts had high catalytic activity and good effects for removing the harmful metal ion in waste water. It was also reported that iron containing activated carbon were active and selective catalysts for phenol oxidation with H_2O_2 as oxidant. It is revealed that iron display better activity than other transition metals [3], although other catalysts, mostly transition metals supported on zeolites and other porous materials, such as TS-1[4, 5] and Ti-MCM-41, were commonly used [6]. However, their wide industrial applications were limited by the high cost with multi-step preparation. So many researchers have studied the performance of activated carbon supported Fe species due to its lower cost[7, 8]. Commercially available activated carbon with high surface area was usually used as support to prepare the catalyst and adsorbent [8, 9]. Impregnation method was the most commonly used for the loading of active components, such as Fe, Cu, etc.[9, 10]. AC could be produced from waste materials such as rice huck lignite by high temperature treatment[11]. Physical and chemical activation methods are fundamentally employed for the preparation of ACs. Physical activation involves reaction at high temperatures in steam or carbon dioxide [12]. In chemical activation, raw material is mixed with an activator, and the mixture was subjected to heat treatment [13, 14]. That is to say, for the preparation of AC-supported catalyst, such as magnetic Fe_3O_4-activated carbon [15], two high temperature steps were included, that is, the preparation of activation carbon involved high temperature process and the loading of iron also encountered high temperature process . If the activation process and iron loading process could be combined in one step, it could reduce the energy consumption in the preparation of iron loaded carbon from agricultural waste. In the present work, PC, the by-product of bio oil production by pyrolysis, was used to produce Fe/activated carbon by an improved method.

2. Experimental

2.1 Preparation of Fe/ activated carbon

Pyrolytic carbon (PC) was produced from rice husk in a fluidized bed reactor, where the rice husk was exposed to 475 °C for less

than 2 s to get bio-oil for the purpose of energy material [2]. The PC with a particle size of 40–80 mesh was washed by distilled water and then dried at 110 °C for 24 h. Then 30.00 g PC was mixed with 200 mL 3M NaOH aqueous solution and the mixture was kept at 100 °C for 5 h. The mixture was cooled to room temperature and filtered, and the filtrate of sodium silicate solution could be used to produce silica [16]. The residue was washed by water to reach a constant pH of about 7 and dried at 110 °C for 24 h, and was named as PC-b.

5.00 g PC-b was immersed in 70 mL iron solution containing n (the controlled amount) mmol $Fe(NO_3)_3 \cdot 9H_2O$. The mixture was stirried under ultrasonic instrument within 0.5 h. The impregnation was maintained at 70 °C till the complete evaporation of water and then it was dried at 110 °C for 24 h. The dried material (C-Fe) were introduced into a tube reactor and heated from room temperature to the final activation temperature under nitrogen flow of 60 mL min^{-1}. The samples were kept at the final temperature for 1.5 h before cooling down to room temperature. The activation temperatures used were 400 °C, 500 °C, 550 °C, 650 °C, 750 °C, and 850 °C. The resultant samples were denoted as C-Fe-y-z (y was the activation temperature, °C, z was iron content mmol/g).

2.2 Characterization of the samples

PC and iron impregnated carbon (C-Fe) were heated at a rate of 5 °C min^{-1}, from room temperature to 800 °C in nitrogen flow. The evolved gas was analyzed by mass spectrometry (MS). CO_2 arising from the oxidation of the sample was monitored by recording the m/z = 44 signal. NO arising from the reactive decomposition of $Fe(NO_3)_3$ was monitored by recording the m/z = 30 signal. H_2O and NO_2 were monitored by recording the m/z = 18 signal and 46 signal, respectively.

IRIS Advantage ICP-AES was used to analyze the amount of metal elements contained in the PC and Fe/activated carbon samples. 0.20 g sample was burnt up to ash at 800 °C for 3 h in air. The obtained ash was dissolved in 1:1 hydrochloric acid solution and further diluted to 100 mL by distilled water. Thus, the metal content could be obtained by analyzing the solution [9].

The specific surface area and pore size distributions of the samples were measured by N_2 adsorption at −196 °C using a Micromeritics TriStar 3020 instrument. The BET surface area (S_{BET}) was calculated from N_2 adsorption isotherms by using the BET equation[16]. Micropore volumes (V_{mic}), micropore surface area (S_{mic}) and external surface area (S_{ext}) were calculated using the t-plot method. The average pore diameter was estimated from the surface area and pore volume [9]. Prior to gas adsorption measurements, the samples were degassed at 120 °C for 1.5 h and 300 °C for 2.5 h in vacuum condition until a pressure of less than 10^{-2} Pa.

The XRD measurement was carried out on a DANDONG FANGYUAN DX-1000 instrument with Cu K_α radiation, operated at 40 kV and 25 mA. The diffracted intensity was measured over the 2θ ranged from 5° to 80°.

SEM was used to observe the morphological features of the samples. The experiment was performed on INSPECTF with an acceleration voltage of 20 kV. Samples were coated with gold before measurements.

The X-ray photoelectron spectroscopy (XPS) was performed on a AXIS Ultra DLD (KRATOS) high performance electron spectrometer with Al Ka radiation (1486.6 eV). The Al Ka X-ray source was operated at 25W, and the binding energy (BE) was calibrated using the C 1s peak at 284.5 eV. A Shirly background was substrated from all spectra. The peak fitting was performed with 80/20 Lorentz–Gauss function. The software XPSPEAK41 was employed to fit the peaks of Fe 2p, C 1s and O 1s [17].

2.3 Activity test

The hydroxylation of phenol was carried out in 50 mL two-necked round-bottom flask equipped with reflux condenser and temperature-controlled water bath. The reaction was carried out under the following typical conditions: phenol, 1.00 g; H_2O_2, 1.00 mL; water, 10.00 mL; reaction time, 0.5-10 min; reaction temperature, 30 °C. The pH value of the reaction system was adjusted to about 3 by adding acetic acid. After reaction, the mixture was taken out and filtered. Finally, the liquid phase was analyzed by High Performance Liquid Chromatography (Waters 1525p) equipped with a 2847 ultraviolet detector at 277 and 254 nm using a reverse phase C18 column. The main products were quantified using o-cresol as internal standard, while acetonitrile/water (v/v = 1:9) was used as the mobile phase. The amount of dihydroxyben-zenes (DHB) is the sum of n_{HQ} and n_{CAT}. The conversion of phenol (X_{ph}), the yield of dihydroxybenzenes (Y_{DHB}), the selectivity to dihydroxybenzenes (S_{DHB}), the selectivity to hydroquinone (S_{HQ}), the selectivity to catechol (S_{CAT}), and the selectivity to benzoquinone (S_{BQ}) are defined as follows:

$$X_{ph} = (n_{ph}^0 - n_{ph}) / n_{ph}^0$$

$$Y_{DHB} = (n_{HQ} + n_{CAT}) / n_{ph}^0$$

$$S_{DHB} = (n_{HQ} + n_{CAT}) / (n_{ph}^0 - n_{ph})$$

$$S_{CAT} = n_{CAT} / (n_{ph}^0 - n_{ph})$$

$$S_{HQ} = n_{HQ} / (n_{ph}^0 - n_{ph})$$

$$S_{BQ} = n_{BQ} / (n_{ph}^0 - n_{ph})$$

where n_{Ph}^0 and n_{Ph} denote the initial and final amounts (moles) of phenol, respectively, while n_{HQ}, n_{CAT}, and n_{BQ} denote the produced amounts (moles) of hydroquinone, catechol, and p-benzoquinone, respectively.

3. Results and Discussion

3.1 Characterization of the Samples

3.1.1 TPD-MS of PC and C-Fe

PC and C-Fe were heated from room temperature to 800 °C under nitrogen flow of 10 mL min^{-1}. The gas evolved in the heating process was analysed by mass spectra, and the result was shown in the Fig. 1. In the heating process of PC, H_2O and CO_2 were released. CO_2 was produced at 240-700 °C, while H_2O was released at 30-200 °C. In the heating process of C-Fe, H_2O, CO_2 and NO were released. NO was released at 120-350 °C. At the same times, CO_2 started to emit at about 120 °C for C-Fe, while for PC it started at 240 °C. It was indicated that Fe species interacted with carbon and this kind of interaction made the oxidation of carbon start at much lower temperature. In the heating process of C-Fe, $Fe(NO_3)_3$ could oxidize carbon and

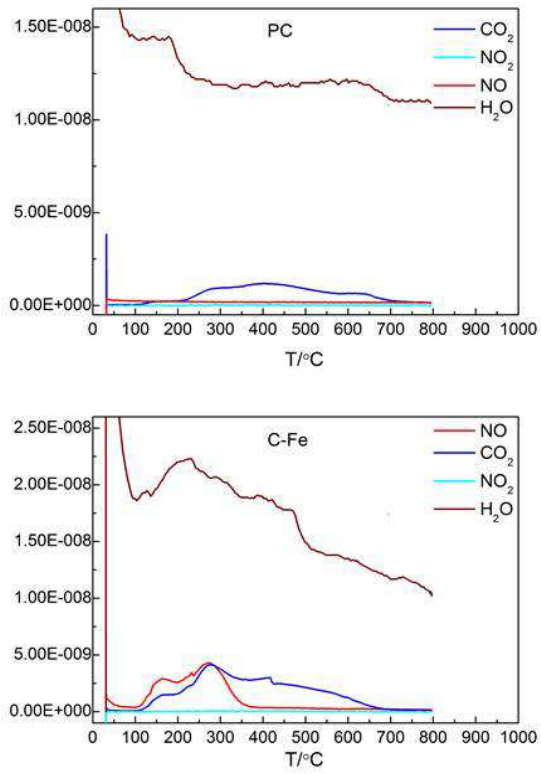

Fig. 1 Analysis of the gas in the heating process of PC and C-Fe

change the properties of activated carbon, creating pore in carbon and generating CO_2, Fe_2O_3 and NO, that is, the reaction (1) occurred. It was reported that the decomposition of nitrate iron on activated carbon started to occur at about 140 °C in air atmosphere, emitting NO_2 [10]. The different result in the nitrogen oxides released might be caused by the atmosphere and substrate used. In previous work, commercially available AC was used and the decomposition of $Fe(NO_3)_3$ occurrred in air atmosphere. No simultaneous formation of CO_2 had been observed. In the present work, $Fe(NO_3)_3$ on the PC reacted with carbon and produced NO and CO_2 at the same time in nitrogen atmosphere. The amount of CO_2 and NO released from C-Fe could be obtained by the peak area. The CO_2 and NO released were 0.481 mmol and 0.273 mmol, respectively. According to the ratio of $Fe(NO_3)_3$ added, the amount of NO_3^- in C-Fe (0.10) was 0.30 mmol, while the amount of NO from the decomposition was 0.273 mmol. These data indicated that NO_3^- decomposed completely in the heating process. Further more, C-Fe was heated from 105 °C to 700 °C by 5 °C/min under nitrogen flow, and the process was also analyzed by TG. The result of TG showed that C-Fe had 30.0 % weight loss. Meanwhile the data were consistent with the sum of CO_2 and NO (29.4 %).

$$4Fe(NO_3)_3(s) + 9C(s) == 2Fe_2O_3(s) + 12NO(g) + 9CO_2(g) \quad (1)$$

3.1.2 The content of Fe and BET

The actual iron contents of the prepared Fe/activated carbon samples were determined by ICP, and the surface area and pore

Table 1 BET of PC and different Fe content Fe/activated carbon samples

sample	Fe content (mmol/g)	A_{BET} (m^2g^{-1})	A_{mic} (m^2g^{-1})	V_{mic} (cm^3g^{-1})	Average pore width(Å)
PC	0	96	77	0.031	24.6
C-Fe-750-0.15	0.15	427	350	0.141	20.9
C-Fe-750-0.39	0.39	527	392	0.160	23.4
C-Fe-750-0.72	0.72	498	396	0.161	21.3
C-Fe-750-1.0	1.0	480	393	0.159	21.3
C-Fe-750-1.3	1.3	434	360	0.146	20.3
C-Fe-750-2.0	2.0	352	234	0.096	35.4

Table 2 BET of different activated temperature Fe/activated carbon samples

sample	T(℃)	A_{BET} (m^2g^{-1})	A_{mic} (m^2g^{-1})	V_{mic} (cm^3g^{-1})	Average pore width(Å)
C-Fe-400-1.0	400	255	180	0.073	26.3
C-Fe-500-1.0	500	358	276	0.112	22.7
C-Fe-550-1.0	550	388	295	0.120	24.0
C-Fe-650-1.0	650	425	352	0.142	20.5
C-Fe-750-1.0	750	480	393	0.159	21.3
C-Fe-850-1.0	850	325	196	0.081	34.1

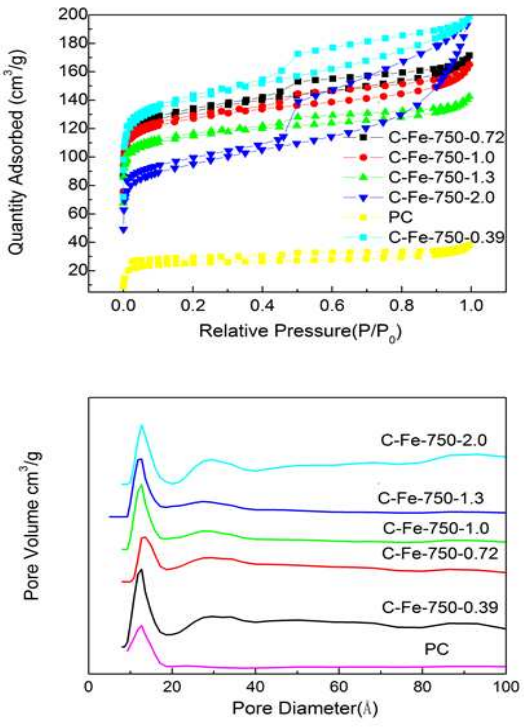

Fig. 2 Adsorption−desorption isotherms of N_2 and pore size distributions for PC and iron-impregnated activated carbon samples

size distribution were determined by BET. The results were listed in Table 1. It was shown that the actual iron content on the samples increased from 0.15 to 2.0 mmol/g. The N_2 adsorption isotherms shown in Fig.2 corresponded to typical type I in the BDDT classification [18], which indicated that all the samples were micropore materials. The hysteresis loops in the nitrogen isotherm represented the existence of some mesopores, and the hysteresis loops of parallel adsorption and desorption branches were indicative of slit-shaped pores [19]. The average pore diameters were between 2.03 nm and 2.46 nm, and the pore size distributions focused on 1.0-1.8 nm mostly, indicative of its micropores character.

Fe species benefited the production of pores on the carbon when the Fe content was low. With the increase of Fe content, the specific surface area of carbon increased first and then decreased, and the maximum specific surface area of 527 m^2g^{-1} was obtained when the Fe content was 0.39 mmol/g. With the increase of the Fe content, S_{BET} , S_{mic}, S_{ext}, and V_{mic} all decreased. The results were most probably due to the consequence of pore blockage after deposition of iron on the mouth of small pores [7].

The BET result of different temperature activated Fe/activated carbon samples were listed in Table 2. With the increase of the activation temperature, the surface area of activated carbon samples increased firstly, reached the maximum at 750 °C, and then decreased. Below 750 °C, the increase of temperature is beneficial to the formation of pores in the carbon. Especially, when the temperature increased from 400 to 500 °C, the surface area of Fe/activated carbon increased obviously from 255 to 358 m^2g^{-1}. This might be caused by the fact that Fe^{3+} was oxidable, while carbon was reducible over this temperature range. The carbon reacted with Fe_2O_3 and produced Fe_3O_4 and CO_2, which was in accordance with the result of mass spectra. With further increase in temperature, the pore was destroyed and it led to the decrease of surface area and expansion of average pore width. High temperature will destroy the structure of carbon, and is not conductive to the pore formation [16]. It is shown that the formation of activated carbon and the loading of Fe is succesfully combined in one step, achieving supported iron catalysts with high specific surface area.

3.1.3 XRD

Fig.3.a displays the XRD patterns of the Fe/activated carbon at different activated temperatures. XRD peaks of iron species could not be detected until the calcination temperature increased up to 400 °C, which indicated that Fe species dispersed highly on activated carbon when calcined at lower temperatures (≤400 °C) [20, 21]. The XRD patterns of C-Fe-70-1.0, C-Fe-110-1.0, and C-Fe-400-1.0 were quite disperse, which was possibly caused by the low content of Fe. On C-Fe-450-1.0, C-Fe-500-1.0 and C-Fe-550-1.0, obvious diffraction peaks were detected at 30.0, 35.5, 44.0 and 57.5°. By comparison with the 2 θ value of the C-Fe-550-1.0 and the patterns of standard magnetite (JCPDS Card No: 19-629), it can be found that all peaks correspond to magnetite Fe_3O_4 were present, and weak characteristic peaks belonging to other iron oxides (Fe_2O_3) were also present. However, it had no typical diffraction peaks of Fe(0) at 45.0 and 65.0° in the XRD patterns [11]. It implied that the reduction reaction (2) occurred at 400-550 °C, and carbon reacted with Fe_2O_3 leading to augment of pores. The result accorded with the BET data, that is, the surface area of C-Fe-450-1.0 increased a lot compared to C-Fe-400-1.0. Fig.3.b indicated that C-Fe-650-1.0 had the peaks of Fe_3O_4. The samples activated above 750 °C exhibited the peaks of metal iron. In the heating process, ferric nitrate took part in a series of reactions and different iron oxides were produced [22, 23]. Fe^{3+} is

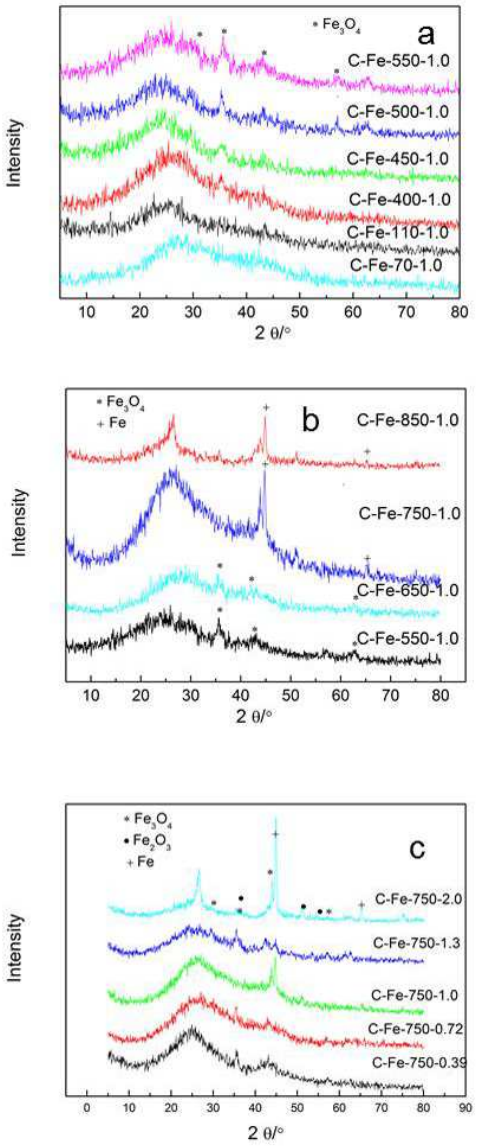

Fig. 3 XRD of the iron-impregnated activated carbon

$$6Fe_2O_3(s)+C(s) == 4Fe_3O_4(s)+CO_2(g) \quad (2)$$

$$2Fe_2O_3(s)+3C(s) == 4Fe(s)+3CO_2(g) \quad (3)$$

$$Fe_3O_4(s)+2C(s) == 3Fe(s)+2CO_2(g) \quad (4)$$

partially reduced to Fe^{2+} and Fe_3O_4 is produced. Fe_3O_4 is further reduced to Fe at 650-750 °C by carbon, that is, the reactions (3) and (4) occurred.

The XRD result of the samples with different iron content activated at 750 °C was presented in Fig. 3.c. The peaks of both Fe_2O_3 and Fe_3O_4 were observed, and with the increase of the iron

Cite this: DOI: 10.1039/c0xx00000x

www.rsc.org/xxxxxx

ARTICLE TYPE

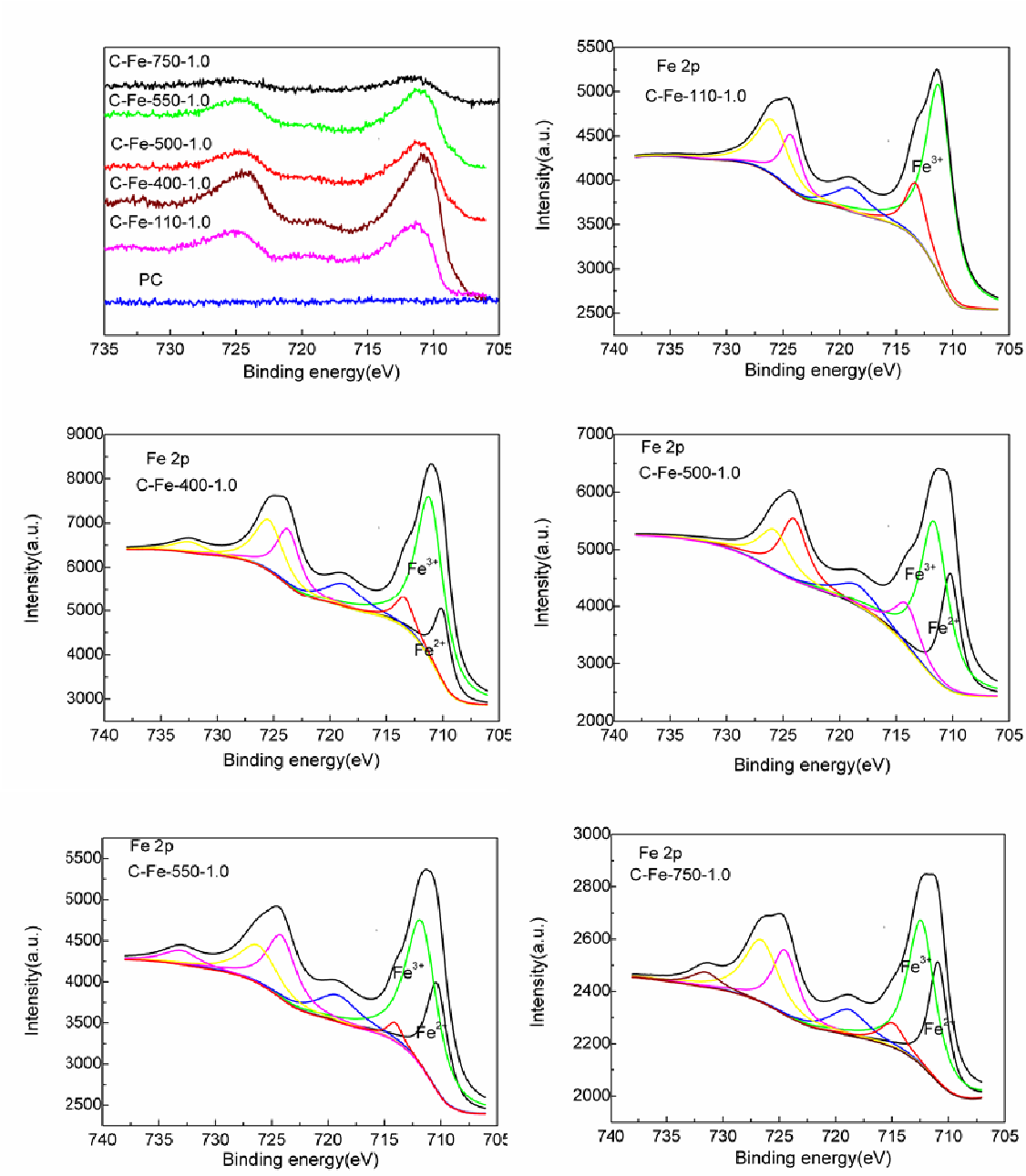

Fig. 4 Fe 2p XPS spectra analysis for iron-impregnated activated carbon samples

content, the diffraction peaks for metal iron appeared. As shown in Fig.3.c, on the C-Fe-750-2.0, obvious diffraction peaks corresponding to metal iron were detected at 45.0 and 65.0 °. With the increase of activated temperature, the peaks of iron metal were more obvious.

3.1.4 XPS

The surface composition and chemical state of Fe in the iron impregnated samples were analyzed by XPS and presented in Fig. 4. All the binding energies were referenced to C 1s at 284.6 eV. As expected, distinct C 1s, O 1s, and Fe 2p peaks are observed in the survey scan spectrum for the samples. There was no peak of iron compound on the PC without ferric nitrate impregnated. On the Fe/activated carbon samples, the typical Fe 2p XPS narrow scan spectrum present two main peaks at 711.2 and 725.0 eV

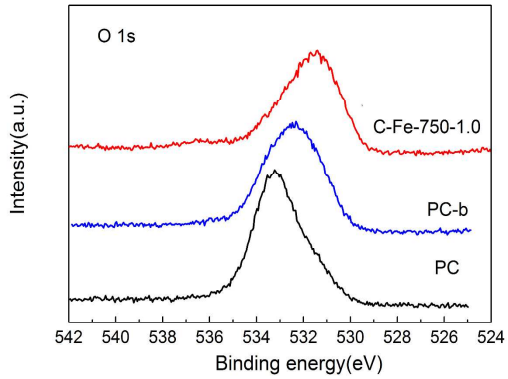

Fig. 5 O 1s XPS spectra analysis for PC, PC-b and C-Fe-750-1.0

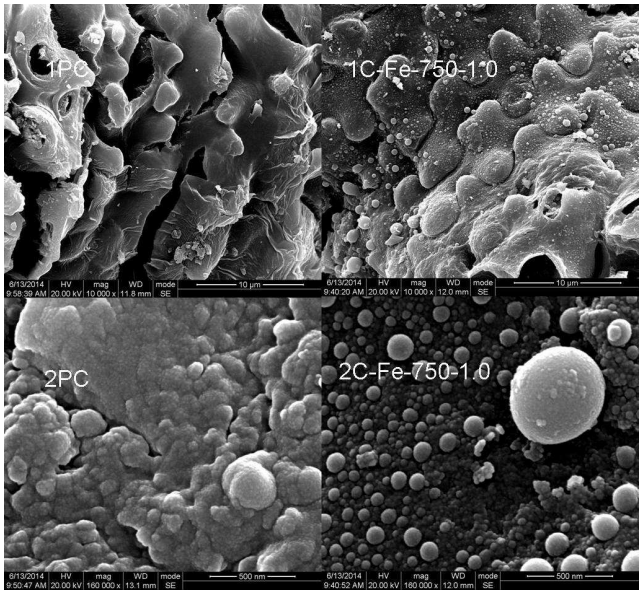

Fig. 6 SEM of the PC and C-Fe-750-1.0

corresponding to the spin-orbit split doublet of Fe $2p_{3/2}$ and Fe $2p_{1/2}$, respectively. The peaks were unsymmetrical, and they were divided into peaks to analyze the ingredient. The peaks at the binding energy of 709.0–710.0 eV, 710.0–712.0 eV, 724.0-725.0 eV and 726.0-727.0 eV were ascribed to Fe^{II} $2p_{3/2}$, Fe^{III} $2p_{3/2}$, Fe^{II} $2p_{1/2}$, and Fe^{III} $2p_{1/2}$. In addition, a satellite peak around 719.0 eV confirmed the presence of Fe^{III} species in the surface of all the samples [7]. The shoulder peak at 714.6 eV might be ascribed to iron ions complexed with electronegative surface ligands [9]. These could be identified as Fe_3O_4.[20, 24]. The C-Fe-110-1.0 was presented in Fig. 4(b), and only the Fe^{III} $2p_{3/2}$ peaks were observed. It implied that the sample was just dried at 110 °C. The O 1s binding energy of 532.5 and 533.7 eV could be assigned to oxygen in SiO_2 impurity (Si=O) and phenol oxygen (C−O). As shown in Fig. 5, the PC has the peak of SiO_2. The peaks of PC-b and C-Fe-750-1.0 were moving to right clearly, and it indicated that the SiO_2 in the PC was removed by NaOH solution effectively. The O 1s peak at 530.3 eV observed on the

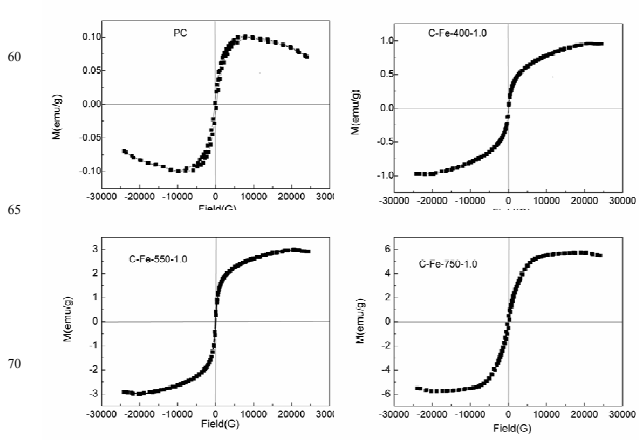

Fig.7 Magnetic hysteresis cycles for the PC and iron impregnated carbon

C-Fe-750-1.0 could be assigned to the Fe−O bond.

3.1.5 SEM

Scanning electron micrography (SEM) was used to perform the morphological examination of the PC and C-Fe-750-1.0 and the result was shown in the Fig. 6. The surface of PC was smooth and there was a lot of small solid particles on C-Fe-750-1.0. It was indicated that iron was loaded on the carbon successfully. It can be seen that the iron oxide particles distributed on the porous structure and covered the surface of activated carbon in the impregnation process.

3.1.6 Magnetism of PC and iron impregnated carbon

The magnetic characterization by a vibrating sample magnetometer (LakeShore 7410) was depicted in Fig. 7. From the plot of magnetization (M) and magnetic field, the PC had very weak hysteresis. It revealed that PC was not a magnetic material and the average saturation magnetization was less than 0.10 emu/g. The saturation magnetization of C-Fe-400-1.0 was 0.97 emu/g. The results indicated that the sample gained magnetic property as a result of the loading of Fe species. The magnetic property was contributed by the presence of Fe_3O_4. The saturation magnetization of C-Fe-550-1.0 and C-Fe-750-1.0 were 2.98 emu/g and 5.73 emu/g, respectively. It indicated that magnetic substance was produced on the carbon with increased activation temperature.

3.2 Catalytic activity studies

3.2.1 Phenol Hydroxylation Reaction

The results were presented in Table 3. All the iron-containing catalysts showed obvious activity for phenol hydroxylation. The yield of dihydroxy benzenes (Y_{DHB}) was low without catalyst at different temperature. The X_{ph} increased with increasing temperature, but the X_{ph} and Y_{DHB} were low without catalysis. Especially, the reaction did not produce HQ under ambient conditions. It was clear that iron was responsible for the activity. As shown in Table 4, with the content of iron on the catalyst increased, the Y_{DHB} increased and then decreased. The C-Fe-750-1.0 exhibits the best activity for the phenol hydroxylation. In Table 5, the effect of the amount of catalyst for phenol hydroxylation was researched. The optimum amount of catalyst was 0.1g and Y_{DHB} could reach 34.0% with S_{DHB} of 65.8%. The

Table 3 Effect of temperature for phenol hydroxylation without catalysis

Catalyst	H_2O_2 (mL)	T(℃)	t (min)	X_{ph} (%)	Y_{DHB} (%)	S_{DHB} (%)	S_{CAT} (%)	S_{HQ} (%)	S_{BQ} (%)
-	1	30	60	5.6	0.0	0.7	0.7	0.00	0.1
-	1	40	60	5.7	0.1	1.1	1.1	0.00	0.4
-	1	50	60	5.4	0.1	1.0	1.0	0.00	0.6
-	1	60	60	6.3	0.1	1.8	1.8	0.00	1.1
-	1	70	60	8.0	0.1	1.3	1.3	0.00	0.7

Table 4 Effect of iron content of catalysis for phenol hydroxylation

Catalyst	Mc (g)	H_2O_2 (mL)	T (℃)	t (min)	X_{ph} (%)	Y_{DHB} (%)	S_{DHB} (%)	S_{CAT} (%)	S_{HQ} (%)	S_{BQ} (%)
C-Fe-750-0.39	0.05	1	30	1	5.5	0.1	2.2	2.2	0.0	0.4
C-Fe-750-0.72	0.05	1	30	1	8.0	3.8	47.8	29.7	18.1	7.2
C-Fe-750-1.0	0.05	1	30	1	52.7	31.4	59.6	33.4	26.2	0.1
C-Fe-750-1.3	0.05	1	30	1	50.9	31.3	61.5	31.1	30.4	0.0
C-Fe-750-2.0	0.05	1	30	1	44.1	25.4	57.5	33.1	24.3	0.1

Table 5 Effect of amount of catalysis for phenol hydroxylation

Catalyst	Mc (g)	H_2O_2 (mL)	T (℃)	t (min)	X_{ph} (%)	Y_{DHB} (%)	S_{DHB} (%)	S_{CAT} (%)	S_{HQ} (%)	S_{BQ} (%)
C-Fe-750-1.0	0.02	1	30	1	42.8	27.5	64.3	39.4	25.0	1.3
C-Fe-750-1.0	0.05	1	30	1	52.7	31.4	59.6	33.4	26.2	0.1
C-Fe-750-1.0	0.10	1	30	1	50.6	33.3	65.8	33.9	31.9	0.1
C-Fe-750-1.0	0.15	1	30	1	50.6	30.2	59.7	31.3	28.3	0.0
C-Fe-750-1.0	0.20	1	30	1	49.7	29.2	58.7	30.2	28.6	0.1

Table 6 Effect of reaction time for phenol hydroxylation

Catalyst	Mc/g	H_2O_2 (mL)	T (℃)	t (min)	X_{ph} (%)	Y_{DHB} (%)	S_{DHB} (%)	S_{CAT} (%)	S_{HQ} (%)	S_{BQ} (%)
C-Fe-750-1.0	0.05	1	30	0.5	29.0	16.8	57.8	36.0	21.8	0.4
C-Fe-750-1.0	0.05	1	30	1	52.7	31.4	59.6	33.4	26.2	0.1
C-Fe-750-1.0	0.05	1	30	3	55.0	32.2	58.5	33.7	24.9	0.1
C-Fe-750-1.0	0.05	1	30	6	56.2	37.0	65.7	37.8	28.0	0.3
C-Fe-750-1.0	0.05	1	30	15	56.4	36.5	64.7	36.6	28.2	0.1

Table 7 Leaching analysis of C-Fe-750-1.0 in the hydroxylation of phenol

Catalyst	H_2O_2 (mL)	T (℃)	t (min)	X_{ph} (%)	Y_{DHB} (%)	S_{DHB} (%)	S_{CAT} (%)	S_{HQ} (%)	S_{BQ} (%)
Leachate	1	30	6	17.6	10.5	59.7	41.2	18.5	12.1
Leached-C	1	30	6	26.4	16.8	63.6	42.2	21.4	6.8

effect of reaction time for phenol hydroxylation was present in Table 6. The C-Fe-750-1.0 exhibited high phenol hydroxylation activity and Y_{DHB} could reach 37.0% within 6 min. With the prolongation of time, Y_{DHB} did not increase further.

In the phenol hydroxylation reaction, an induction period of 5−120 min was previously mentioned in the literature. It was reported that adding a small amount of CH_3COOH could shorten and eliminate the induction period [3, 25, 26]. Many studies have shown that the phenol hydroxylation needed a reaction time of 1-3h, with the phenol conversion of 40-50%, and the selectivity of dihydroxybenzenes is within 70.6-90% [10, 27]. C-Fe-750-1.0 could shorten the reaction time greatly, because of different valence state iron species were produced on the carbon.

It is reported that Fe_3O_4 species present higher catalytic performance than Fe_2O_3 for the activation of H_2O_2 [28]. The preparation of this catalyst from agricultural waste combined activation process and iron loading process to one step. It reduced the energy consumption and produced value added samples.

3.2.2 Leaching analysis

The iron content of C-Fe-750-1.0 after reaction testing and the iron leaching in the reaction solution were analyzed by ICP. The iron content remained on the used catalyst (C-Fe-1) was 0.027 mmol, and nearly one half of iron on activated carbon leached. 0.05 g C-Fe-750-1.0 and 10 mL solvent (H_2O and acetic acid) were carried out in 50 mL two-necked round-bottom flask at 30 °C. Then, the mixture was taken out and filtered. The carbon (Leached-C) obtained after removal of all leachable sites, as well as the leachates [29]. The Leached-C and Leachate catalyzed the

hydroxylation of phenol, in the same conditions, respectively. As shown in Table.7, the reaction activity was mainly influenced by Leached-C, that is, the heterogeneous catalyst contributed higher activity than the leached species in the solution.

4. Conclusion

The combination of the formation of porous structure with high surface area of activated carbon and the loading of iron in one-step to prepare Fe/activated carbon was realized using rice husk pyrolytic carbon as starting material. The carbon reacted with $Fe(NO_3)_3$, and generated CO_2, Fe_2O_3 and NO below 400°C. Fe_3O_4 dispersed on activated carbon was formed when iron impregnated carbon was activated at 400-550 °C under nitrogen. With higher activation temperature, Fe^{3+} could be reduced to Fe on the carbon. The thus-obtained Fe/activated carbon was very active in the hydroxylation of phenol at 30 °C. Under optimal reaction conditions, a phenol conversion of 56.2 % and a yield of 37.0 % to dihydoxybenzenes were obtained at a short reaction time of 6 min.

Acknowledgements

This work is supported by the National High Technology Research and Development Program (863 program 2012 AA 051803) of China, and NNSFC (No. 21372167). The characterization of the samples by the Analytic and Testing Center of Sichuan University is acknowledged.

Notes and references

Key Laboratory of Green Chemistry and Technology, Ministry of Education, College of Chemistry, Sichuan University, Chengdu, Sichuan, 610064, China. Tel: +86-28-85411105; Fax: +86-28-85411105; E-mail: G. Y. Li: gchem@scu.edu.cn, C. W. Hu: chwehu@mail.sc.cninfo.net, changweihu@scu.edu.cn

* The author was corresponding authors.

1. L. Wang, Y. Guo, Y. Zhu, Y. Li, Y. Qu, C. Rong, X. Ma and Z. Wang, *Bioresour. Technol.*, 2010, **101**, 9807-9810.
2. Q. Lu, X. Yang and X. Zhu, *J. Anal. Appl. Pyrolysis*, 2008, **82**, 191-198.
3. J.-S. Choi, S.-S. Yoon, S.-H. Jang and W.-S. Ahn, *Catalysis Today*, 2006, **111**, 280-287.
4. P. Chammingkwan, W. F. Hoelderich, T. Mongkhonsi and P. Kanchanawanichakul, *Applied Catalysis A: General*, 2009, **352**, 1-9.
5. X. Ke, L. Xu, C. Zeng, L. Zhang and N. Xu, *Microporous and Mesoporous Materials*, 2007, **106**, 68-75.
6. K. Lin, L. Wang, F. Meng, Z. Sun, Q. Yang, Y. Cui, D. Jiang and F. Xiao, *Journal of Catalysis*, 2005, **235**, 423-427.
7. A. Rey, M. Faraldos, J. A. Casas, J. A. Zazo, A. Bahamonde and J. J. Rodríguez, *Applied Catalysis B: Environmental*, 2009, **86**, 69-77.
8. W. Ling, Z. Qiang, Y. Shi, T. Zhang and B. Dong, *Journal of Molecular Catalysis A: Chemical*, 2011, **342-343**, 23-29.
9. H. Liu, G. Li and C. Hu, *J. Mol. Catal. A: Chem.*, 2013, **377**, 143-153.
10. M. Jin, R. Yang, M. Zhao, G. Li and C. Hu, *Industrial & Engineering Chemistry Research*, 2014, **53**, 2932-2939.
11. T. Depci, *Chemical Engineering Journal*, 2012, **181-182**, 467-478.
12. V. Subramanian, C. Luo, A. M. Stephan, K. S. Nahm, S. Thomas and B. Wei, *J. Phys. Chem. C*, 2007, **111**, 7527-7531.
13. M. A. Lillo-Rodenas, D. Cazorla-Amoros and A. Linares-Solano, *Carbon* 2003, **41**, 267-275.
14. Y. Guo, S. Yang, K. Yu, J. Zhao, Z. Wang and H. Xu, *Mater. Chem. Phys.*, 2002, **74**, 320-323.
15. N. Yang, S. Zhu, D. Zhang and S. Xu, *Materials Letters*, 2008, **62**, 645-647.
16. Y. Liu, Y. Guo, W. Gao, Z. Wang, Y. Ma and Z. Wang, *J. Cleaner Prod.*, 2012, **32**, 204-209.
17. X. Liang, R. Yang, G. Li and C. Hu, *Microporous and Mesoporous Materials*, 2013, **182**, 62-72.
18. S. Brunauer, L. S. Deming, W. E. Deming and E. teller, *J. Am. Chem. Soc.*, 1940, **62**, 1723-1732.
19. H. H. Tseng, M. Y. Wey and C. H. Fu, *Carbon*, 2003, **41**, 139-149.
20. S. Song, H. Yang, R. Rao, H. Liu and A. Zhang, *Applied Catalysis A: General*, 2010, **375**, 265-271.
21. J. Choi, T. Kim, K. Choo, J. Sung, M. Saidutta, S. Ryu, S. Song, B. Ramachandra and Y. Rhee, *Applied Catalysis A: General*, 2005, **290**, 1-8.
22. J. D. Desai, H. M. Pathan, S.-K. Min, K.-D. Jung and O.-S. Joo, *Applied Surface Science*, 2006, **252**, 8039-8042.
23. J. D. Desai, H. M. Pathan, S.-K. Min, K.-D. Jung and O.-S. Joo, *Applied Surface Science*, 2006, **252**, 2251-2258.
24. T. Missana, C. Maffiotte and M. García-Gutiérrez, *Journal of Colloid and Interface Science*, 2003, **261**, 154-160.
25. G. M. S. R. O. Rocha, R. A. W. Johnstone and M. G. P. M. S. Neves, *Journal of Molecular Catalysis A: Chemical* 2002, **187**, 95-104.
26. C. Xiong, Q. Chen, W. Lu, H. Gao, W. Lu and Z. Gao, *Catalysis Letters*, 2000, **69**, 231-236.
27. S. Yang, G. Liang, A. Gu and H. Mao, *Applied Surface Science*, 2013, **285p**, 721-726.
28. W. F. d. Souza, I. R. G. aes, L. C. A. Oliveira, M. a. C. Guerreiro, A. L. N. Guarieiro and K. T. G. Carvalho, *Journal of Molecular Catalysis A: Chemical* 2007, **278**, 145-151.
29. C. A. Deshmane, M. W. Wright, A. Lachgar, M. Rohlfing, Z. Liu, J. Le and B. E. Hanson, *Bioresour. Technol.*, 2013, **147**, 597-604